Available online at www.sciencedirect.com
SCIENCE DIRECT®
Advances in Water Resources 27 (2004) 129–140
Advances in Water Resources
www.elsevier.com/locate/advwatres

Application of the discontinuous spectral Galerkin method to groundwater flow

Sergio Fagherazzi [a,*], David Jon Furbish [b,1], Patrick Rasetarinera [c,2], M. Youssuff Hussaini [c]

[a] Department of Geological Sciences and School of Computational Science and Information Technology, Dirac Science Library, Florida State University, Tallahassee, FL 32306-4120, USA
[b] Department of Geological Sciences and Geophysical Fluid Dynamics Institute, Florida State University, Tallahassee, USA
[c] School of Computational Science and Information Technology, Florida State University, Tallahassee, USA

Received 25 November 2002; received in revised form 11 November 2003; accepted 11 November 2003

Abstract

The discontinuous spectral Galerkin method uses a finite-element discretization of the groundwater flow domain with basis functions of arbitrary order in each element. The independent choice of the basis functions in each element permits discontinuities in transmissivity in the flow domain. This formulation is shown to be of high order accuracy and particularly suitable for accurately calculating the flow field in porous media. Simulations are presented in terms of streamlines in a bidimensional aquifer, and compared with the solution calculated with a standard finite-element method and a mixed finite-element method. Numerical simulations show that the discontinuous spectral Galerkin approximation is more efficient than the standard finite-element method (in computing fluxes and streamlines/pathlines) for a given accuracy, and it is more accurate on a given grid. On the other hand the mixed finite-element method ensures the continuity of the fluxes at the cell boundaries and it is particular efficient in representing complicated flow fields with few mesh points. Simulations show that the mixed finite-element method is superior to the discontinuous spectral Galerkin method producing accurate streamlines even if few computational nodes are used. The application of the discontinuous Galerkin method is thus of interest in groundwater problems only when high order and extremely accurate solutions are needed.

Keywords: Groundwater flow; Groundwater streamlines; Discontinuous Galerkin; Spectral methods; Discontinuous transmissivity

1. Introduction

Numerical simulations are widely used in characterizing subsurface flows. They are normally based on low order finite-element or finite-difference approximations [6,32] as they are robust and easy to implement. The common approach is first to calculate the distribution of the potential head from the equation of conservation of mass and then to derive discharges through the Darcy fluxes. Following this approach, in the finite-difference method the head at the center of a cell is computed applying a water balance over the cell boundaries. In this way the flux normal to a finite-difference cell side is continuous and it is possible to compute flux-conserving path lines [33]. When complex geometries and flow fields are modeled, finite elements generally provide more flexibility than finite differences. However, when linear triangular elements are used, the head is approximated as varying linearly in each element leading to a constant discharge. As a consequence, fluxes across element boundaries are discontinuous and path lines derived from these fluxes may be of low accuracy [22].

As high accuracy of fluxes is essential for simulating transport in heterogeneous porous formations [5,36], improving the flux approximation in finite-element models has been approached in several ways. A dual formulation of the flow, utilizing both potential and stream functions, leads to better results [22]. In a steady

* Corresponding author. Tel.: +1-850-644-7022; fax: +1-850-644-0098.
E-mail address: sergio@csit.fsu.edu (S. Fagherazzi).
[1] Present address: Department of Earth and Environmental Sciences, Vanderbilt University, Nashville, TN 37235-1085, USA.
[2] Present address: Cadence Design Systems, Inc. 2655, Seely Avenue San Jose, CA 95134, USA.

0309-1708/$ - see front matter © 2004 Elsevier Ltd. All rights reserved.
doi:10.1016/j.advwatres.2003.11.001

flow, both the head equation and the streamline equation are solved together, and the knowledge of the stream function allows the calculation of streamlines. The dual formulation has been extended to domains that include wells and stagnation points [13], and to three-dimensional flow fields [27]. Unfortunately, the steady-state constraint makes the dual formulation unsuitable for modeling transient phenomena.

Another approach introduced by Cordes and Kinzelbach [19] consists of postprocessing the head distribution obtained from standard finite-element methods. This can be achieved by imposing the continuity and the irrotationality conditions on subelements obtained from the finite-element discretization and taking into account that the conforming finite-element method gives an exact water balance at every node. This procedure yields a continuous flux distribution and accurate streamlines over the domain.

A third approach relies on mixed finite-element methods. Following Meissner [28], for example, both head and fluxes are independently considered. As the resulting large system of linear equations leads to a matrix that is not positive definite, hybridization has been utilized [4,12]. Mosé et al. [29] recently compared this method with the Cordes and Kinzelbach postprocessor and showed that the mixed finite-element method is superior in terms of flux distribution accuracy, particularly in the presence of strong heterogeneity in transmissivity. (For a discussion of the general validity of these results, see also [20].) However, due to the greater number of unknowns, mixed hybrid finite-element methods require more memory and computation time, although they provide physically more realistic solutions to the flow field in very discontinuous and heterogeneous systems [21]. All these methods are of low order, whereas the study of complex physics with computing constraints requires higher-order methods.

Goblet and Cordier [23] appear to be among the first to have used a higher-order method of spectral accuracy in a hydrological context. They solved the two-dimensional flow and mass transport equations with the so-called spectral element method, which is essentially due to Patera and his colleagues ([31] see also, for example, [24]). In this method, the domain of computation is subdivided into elements of uniform order. The method permits the solution in each element to be approximated to an arbitrary order of accuracy. The choice of spectral basis functions in each element, such as the Legendre polynomials that the authors have used, ensures the approximation error to decay exponentially. Globet and Cordier [23] employed polynomials of order up to eight and demonstrated the high order accuracy and efficiency of the spectral element method in resolving steep gradients and moving fronts.

Recently, another class of methods known as the discontinuous Galerkin methods have become increasingly popular in fluid mechanics, acoustics and electromagnetics ([26,30,34] and others). Modern developments in these methods are primarily due to Cockburn and Shu and their group [14–16]. The key feature is the independent choice of basis functions in each element, which enables adaptive mesh refinement as well as arbitrary order of approximation in each element. In a hydrological context, Aizinger et al. [2] applied the method to the study of groundwater contaminant transport. Specifically, they used the local discontinuous Galerkin (LDG) method of Cockburn and Shu [17] with third-order Runge–Kutta time discretization and spatial discretization based on piecewise constant, linear and quadratic approximations. They mainly considered unsteady one-dimensional transport of one and two-component contaminants. Their conclusion is that "in general the higher degree polynomials give a more accurate solution with smaller CPU time". On the other hand, Riviere et al. [35] applied the formulation of Oden et al. [30] to the steady flow in porous media governed by an elliptic equation with discontinuous diffusivity coefficients. They used polynomials of order up to eight and exploited the adaptive mesh refinement strategy permitted by the method to obtain optimal convergence rates unattainable with a uniform mesh refinement methodology.

In this paper, we apply the local discontinuous spectral Galerkin method (LDG) developed by Cockburn and Shu [14] to the unsteady saturated groundwater flow problem. Specifically, we investigate the performance of the method in a series of numerical tests and compare the results with the standard finite-element and mixed finite-element solutions.

2. The local discontinuous Galerkin formulation

The LDG formulation is applied to the two-dimensional transient flow equations in an aquifer:

$$\frac{\partial q_x}{\partial x}+\frac{\partial q_y}{\partial y}=-S\frac{\partial h}{\partial t}+Q \tag{1}$$

$$q_x=-T_x\frac{\partial h}{\partial x},\quad q_y=-T_y\frac{\partial h}{\partial y} \tag{2}$$

where (1) enforces mass conservation and (2) are the Darcy fluxes. In these equations h represents the hydraulic head, q_x and q_y the discharge per unit width of the aquifer in the x- and y-direction, T_x, T_y are the components of the anisotropic coefficient of hydraulic transmissivity, S is the storage coefficient of the aquifer and Q is the distributed source or sink term.

We descritize the system (1) and (2) by the LDG method (see [17]). The domain is divided into non-overlapping quadrilaterals. We then seek an approximation of the head and discharges belonging to the

space of polynomials of order n (at most) in each element. Multiplying (1) and (2) by an arbitrary smooth function v', and integrating over each element of the triangulation, we obtain, after integration by parts, the following weak formulation for each element E:

$$\int_E \left(S\frac{\partial h}{\partial t} - Q\right)v' \,\mathrm{d}A - \int_E \left(q_x\frac{\partial v'}{\partial x} + q_y\frac{\partial v'}{\partial y}\right)\mathrm{d}A + \int_{\partial E}(\hat{q}_x n_x + \hat{q}_y n_y)v' \,\mathrm{d}\Gamma = 0 \tag{3}$$

$$\int_E \frac{1}{T_x}q_x v' \,\mathrm{d}A - \int_E h\frac{\partial v'}{\partial x}\mathrm{d}A + \int_{\partial E}\hat{h}n_x v' \,\mathrm{d}\Gamma = 0 \tag{4}$$

$$\int_E \frac{1}{T_y}q_y v' \,\mathrm{d}A - \int_E h\frac{\partial v'}{\partial y}\mathrm{d}A + \int_{\partial E}\hat{h}n_y v' \,\mathrm{d}\Gamma = 0 \quad \forall v' \tag{5}$$

where (n_x, n_y) is the outward unit normal to the boundary of the element E, A the element area, and Γ the element boundary. The terms $\hat{q}_x$, $\hat{q}_y$, and $\hat{h}$ on the left-hand side of Eqs. (3)–(5) are numerical fluxes at the edges that link the elements together. Because we want to model abrupt changes in transmissivity at the edges of elements, the quantities T_x and T_y are incorporated within the first integrals of Eqs. (4) and (5).

The major advantage of this scheme is that the basis functions, used to solve the weak formulation (3)–(5), are locally defined for each element. In fact the basis functions are identically zero outside the element, so that we can freely modify the order of the approximation, without modifying the basis functions in other elements. This formulation is thus different from the standard finite-element method where each basis function is defined in all the elements sharing a node, thus enforcing the continuity of the solution. Contrary to the LDG method, in standard finite elements the order of the approximation cannot be changed once the basis functions are chosen.

3. Expansion bases

The first step in resolving the system (3)–(5) is to transform the generic quadrilateral region into the reference square Ω (cf. Fig. 1). If the form of the mapping is known, i.e. we know the two functions X, Y for which $x = X(\xi, \eta)$ and $y = Y(\xi, \eta)$, the system (3)–(5) becomes (e.g. [25]):

$$\int_\Omega \left(S\frac{\partial h}{\partial t} - Q\right)v|J| \,\mathrm{d}A = \int_\Omega (q_x\psi_x + q_y\psi_y)\,\mathrm{d}A + \int_{\partial\Omega}(\hat{q}_x\bar{n}_x - \hat{q}_y\bar{n}_y)v \,\mathrm{d}\Gamma \tag{6}$$

$$\int_\Omega \frac{1}{T_x}q_x v|J| \,\mathrm{d}A = \int_\Omega h\psi_x \,\mathrm{d}A - \int_{\partial\Omega}\hat{h}\bar{n}_x v \,\mathrm{d}\Gamma = 0 \tag{7}$$

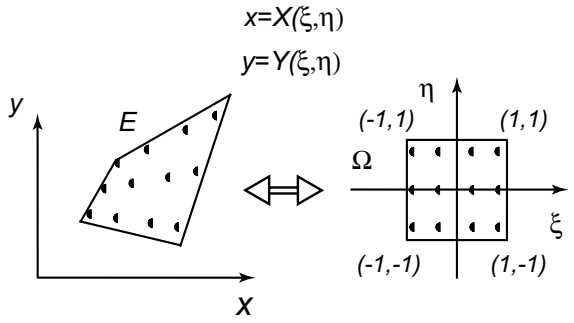

Fig. 1. Transformation of the generic quadrilateral in the reference square. The dots are the Gauss–Legendre points where the head and the discharges are evaluated.

$$\int_\Omega \frac{1}{T_y}q_y v|J| \,\mathrm{d}A = \int_\Omega h\psi_y \,\mathrm{d}A - \int_{\partial\Omega}\hat{h}\bar{n}_y v \,\mathrm{d}\Gamma = 0 \quad \forall v \tag{8}$$

where the Jacobian J and the expressions ψ_x and ψ_y are:

$$J = \frac{\partial X}{\partial\xi}\frac{\partial Y}{\partial\eta} - \frac{\partial X}{\partial\eta}\frac{\partial Y}{\partial\xi}, \quad \psi_x = \frac{\partial v}{\partial\xi}\frac{\partial Y}{\partial\eta} - \frac{\partial v}{\partial\eta}\frac{\partial Y}{\partial\xi}, \quad \psi_y = \frac{\partial v}{\partial\eta}\frac{\partial X}{\partial\xi} - \frac{\partial v}{\partial\xi}\frac{\partial X}{\partial\eta} \tag{9}$$

with v the reference basis function in Ω and the vector $(\bar{n}_x, \bar{n}_y)$ the normal to the boundary of the element E. $(\bar{n}_x, \bar{n}_y)$ is not unity, but rather has length equal to half the side of the element E in consideration. Standard finite-element functions are often used for the mapping X, Y of a reference element.

For each quadrilateral element, we choose independently an order $n \times m$, which means that we evaluate the head and the discharges at $n + 1$ nodes in the x-direction and at $m + 1$ nodes in the y-direction. We choose the nodes (ξ_i, η_j) in the reference square so that they correspond to the Gauss–Legendre points (Fig. 1) (see [1]). The nodes (ξ_i, η_j) are then mapped in (x_i, y_j) in each quadrilateral of the mesh by using the functions X and Y.

As in Goblet and Cordier [23], each base expansion is a tensor product of Lagrange polynomials on the reference domain Ω. The head and the discharges are expressed as:

$$\begin{pmatrix} h \\ q_x \\ q_y \end{pmatrix} = \sum_{j=0}^{m}\sum_{i=0}^{n}\begin{pmatrix} \mathbf{H}_{ij} \\ \mathbf{QX}_{ij} \\ \mathbf{QY}_{ij} \end{pmatrix} L_i^n(\xi)L_j^m(\eta) \tag{10}$$

where $\mathbf{H}_{ij}$, $\mathbf{QX}_{ij}$, and $\mathbf{QY}_{ij}$ are the coefficients of the expansion (10) at the points (ξ_i, η_j) in the reference square. $L_i^n(\xi)$ is the Lagrange polynomial which takes a value of one at the node ξ_i and zero at the others. It can be written as:

$$L_i^n(\xi) = \prod_{j=0, n\, j\neq i}\frac{(\xi - \xi_i)}{(\xi_i - \xi_j)} \tag{11}$$

Because we use Lagrange polynomials the elements of the matrix $\mathbf{H}_{ij}$, $\mathbf{QX}_{ij}$, $\mathbf{QY}_{ij}$ are respectively the values of the head, the x-component and the y-component of the discharge at the points (x_i, y_j), mapped in (ξ_i, η_j) within the reference square. For every element Eqs. (6)–(8) are written $(n+1)\times(m+1)$ times, once for each test function v_{kl}. In the Galerkin formulation these test functions are equivalent to the expansion bases:

$$v_{kl} = L_k^n(\xi)L_l^m(\eta), \quad k = 0, n, \quad l = 0, m \tag{12}$$

4. Numerical integration and differentiation

Since the points ξ_i and η_i correspond to the Gauss–Legendre quadrature points, we can substitute the integrals in (6)–(8) with a weighted sum of the values of the integrand at the quadrature points. Because of the particular choice of the points, this substitution is exact for polynomials with order up to $2n+1$, if $n+1$ is the number of points. The weight w_i^n utilized in the sum can be calculated from available algorithms [8]. Remembering that $L_i^n(\xi_i) = 1$ and $L_i^n(\xi_j) = 0$, for $i \neq j$, integration of the product of Lagrange polynomials evaluated on the Gauss–Legendre points yields the simple result:

$$\begin{aligned}\int_\Omega f(\xi,\eta)L_k^n(\xi)L_l^m(\eta)\,\mathrm{d}A &\simeq \sum_{j=0}^{m} w_j^m \left\{ \sum_{i=0}^{n} w_i^n f(\xi_i,\eta_j)L_k^n(\xi_i)L_l^m(\eta_j)\right\}\\ &= w_k^n w_l^m f(\xi_k,\eta_l)\end{aligned} \tag{13}$$

where w_k^n and w_l^m are the Gauss–Legendre quadrature weights for n and m points respectively. If we consider a constant transmissivity in each element and if we utilize (13) to calculate the left-hand side of (7), we get the following expression:

$$\begin{aligned}\frac{1}{T_x}\int_\Omega q_x v|J|\,\mathrm{d}A &= \frac{1}{T_x}\int_\Omega \left(\sum_{j=0}^{m}\sum_{i=0}^{n}\mathbf{QX}_{ij}(t)L_i^n(\xi)L_j^m(\eta)\right)\\ &\quad\times L_k^n(\xi)L_l^m(\eta)|J|\,\mathrm{d}A\\ &\simeq \frac{1}{T_x}\mathbf{QX}_{kl}w_k^n w_l^m|J(\xi_k,\eta_l)|\end{aligned} \tag{14}$$

In order to calculate the first integral on the right-hand side of Eqs. (6)–(8), we need to obtain a partial derivative of the test function. In spectral methods the derivative of a function is expressed as a matrix-vector multiplication. In our case the test function $v = v_{kl}$ is expanded in Lagrange polynomials and the matrix-vector multiplication simplifies further to:

$$\left.\frac{\partial v_{kl}}{\partial\eta}\right|_{\xi_i,\eta_j} = L_k^n(\xi)\left.\frac{\mathrm{d}}{\mathrm{d}\eta}L_l^m(\eta)\right|_{\xi_i,\eta_j} = \begin{cases}\mathbf{D}_{jl}^m & \text{if } i = k\\ 0 & \text{if } i \neq k\end{cases} \tag{15}$$

where the derivative matrices $\mathbf{D}_{ij}^m$ and $\mathbf{D}_{ij}^n$ are defined as:

$$\mathbf{D}_{ij}^m = L_j^{m'}(\eta_i), \quad \mathbf{D}_{ij}^n = L_j^{n'}(\xi_i) \tag{16}$$

In (16) $L_j^{m'}(\eta)$ is the first derivative of the Lagrange polynomial $L_j^m(\eta)$ and can be calculated only once at the beginning of the simulation [8]. Utilizing (13) and (15) we can now calculate the first term on the right-hand side of Eqs. (6)–(8). For example, for Eq. (7), it becomes:

$$\begin{aligned}\int_\Omega h\psi_x\,\mathrm{d}A \simeq w_l^m \sum_{p=0}^{n}\left\{w_p^n\mathbf{D}_{pk}\mathbf{H}_{pl}\frac{\partial Y}{\partial\eta}(\xi_p,\eta_l)\right\}\\ - w_k^n\sum_{p=0}^{m}\left\{w_p^m\mathbf{D}_{pl}\mathbf{H}_{kp}\frac{\partial Y}{\partial\xi}(\xi_k,\eta_p)\right\}\end{aligned} \tag{17}$$

5. Numerical fluxes and boundary conditions

When the boundary integrals in Eqs. (3)–(5) are evaluated, the terms $\hat{h}$, $\hat{q}_x$, $\hat{q}_y$, which are the fluxes of the head and discharges through the interface, are not uniquely defined due to the discontinuous function approximation. It is therefore necessary to substitute these terms with a numerical flux function, which in general depends on both the states at the left and right of the interface and which introduces a coupling between the unknowns of neighboring elements. Several numerical fluxes have been defined for parabolic and elliptic problems [3,7,17], and their choice is crucial for the stability of the method.

In this paper we adopt the formulation of Cockburn and Shu [17] (see also [3,11]). For each edge separating two elements (called here element 1 and 2) we define the following quantities (the index 1 refers to quantities calculated within the element 1 and the index 2 refers to quantities calculated within the element 2):

$$\begin{aligned}&\{h\} = \tfrac{1}{2}(h_1 + h_2), \quad \{\mathbf{q}\} = \tfrac{1}{2}(\mathbf{q}_1 + \mathbf{q}_2),\\ &[\mathbf{h}] = h_1\mathbf{n_1} + h_2\mathbf{n_2}, \quad [q] = \mathbf{q_1}\cdot\mathbf{n_1} + \mathbf{q_2}\cdot\mathbf{n_2}\end{aligned} \tag{18}$$

with $\mathbf{q} = (q_1, q_2)$, $\mathbf{n_1}$ and $\mathbf{n_2}$ the normals to the edge directed outward the element 1 and 2 respectively. The numerical fluxes are then:

$$\hat{h} = \{h\} + \gamma\cdot[\mathbf{h}], \quad \hat{\mathbf{q}} = \{\mathbf{q}\} - \beta[q] \tag{19}$$

where $\hat{\mathbf{q}}$, and γ are vector valued functions. Here we set $\beta = 1$ and $\gamma = (1,1)$ in order to obtain an optimal convergence rate, as theoretically demonstrated by Castillo et al. [11]. The terms containing β and γ play a role similar to the introduction of numerical diffusion at the boundaries stabilizing the method. Without these terms all the fluxes are the simple average between the values at the two boundaries.

The quantities h_1, h_2, q_1, q_2 are calculated projecting the solution within the element on the edge of the element itself. Since the approximation is a high order

polynomial, the projection is simply a polynomial interpolation. It is necessary to determine the value of the quantities at the same points for both sides before calculating $\{h\}$, $[h]$, $\{\mathbf{q}\}$, $[\mathbf{q}]$, in order to do that we choose a number of points on the edge equal to the lowest of the polynomial orders of the two contiguous elements. The line integrals in (6)–(8) are then computed using the Gauss–Legendre quadrature weights.

In order to resolve the system of Eqs. (3)–(5) suitable boundary conditions are added. Neumann boundary conditions are implemented directly in Eq. (3) substituting the integral at the boundaries with the value of the given flux. The Dirichlet boundary condition is instead utilized in Eqs. (4) and (5) to compute the numerical flux $\hat{h}$. In this way the value of the head at the boundaries is weakly enforced, differently from finite-element and finite-difference methods.

6. Model implementation

The model implementation is fully explicit and does not require the solution of a linear system. Given the current values of the potential head, it is possible to compute the discharge from Eqs. (7) and (8), calculating the integral on the left-hand side and the first integral on the right-hand side as showed in Eqs. (14) and (17), and the numerical flux in the second integral on the right-hand side of Eqs. (7) and (8) using (19). The discharges at the time step n can then be written as: $\mathbf{QX}_{ij}^n = f_1(\mathbf{H}_{ij}^n)$ and $\mathbf{QY}_{ij}^n = f_2(\mathbf{H}_{ij}^n)$ with the operators f_1 and f_2 fully explicit. Once the discharges are calculated it is possible to determine the numerical fluxes $\hat{q}_x$ and $\hat{q}_y$. Eq. (6) is then utilized to calculate the head distribution at the next time step $n+1$, yielding $\mathbf{H}_{ij}^{n+1} = \mathbf{H}_{ij}^n + \Delta t g(\mathbf{QX}_{ij}^n, \mathbf{QY}_{ij}^n)$ with the operator g derived from (6).

To improve the accuracy of the solution at the next time step a Runge–Kutta scheme of the third order is utilized for the time discretization [39]. Following this scheme the discharges and the potential head are computed three times for each time step in order to get the value of the head $\mathbf{H}_{ij}^{n+1}$. The scheme is:

$$\begin{aligned}
&\mathbf{QX}_{ij}^n = f_1(\mathbf{H}_{ij}^n), \quad \mathbf{QY}_{ij}^n = f_2(\mathbf{H}_{ij}^n)\\
&\mathbf{H}_{ij}^{(1)} = \mathbf{H}_{ij}^n + \Delta t g(\mathbf{QX}_{ij}^n, \mathbf{QY}_{ij}^n)\\
&\mathbf{QX}_{ij}^{(1)} = f_1(\mathbf{H}_{ij}^{(1)}), \quad \mathbf{QY}_{ij}^{(1)} = f_2(\mathbf{H}_{ij}^{(1)})\\
&\mathbf{H}_{ij}^{(2)} = \tfrac{3}{4}\mathbf{H}_{ij}^n + \tfrac{1}{4}\mathbf{H}_{ij}^{(1)} + \Delta t g(\mathbf{QX}_{ij}^{(1)}, \mathbf{QY}_{ij}^{(1)})\\
&\mathbf{QX}_{ij}^{(2)} = f_1(\mathbf{H}_{ij}^{(2)}), \quad \mathbf{QY}_{ij}^{(2)} = f_2(\mathbf{H}_{ij}^{(2)})\\
&\mathbf{H}_{ij}^{n+1} = \tfrac{1}{3}\mathbf{H}_{ij}^n + \tfrac{2}{3}\mathbf{H}_{ij}^{(2)} + \Delta t g(\mathbf{QX}_{ij}^{(2)}, \mathbf{QY}_{ij}^{(2)})
\end{aligned} \tag{20}$$

where (1) and (2) indicate the quantities calculated at the two intermediate steps. We note that only the matrix of the head at the steps $\mathbf{H}_{ij}^{(1)}$ and $\mathbf{H}_{ij}^{(2)}$ has to be stored and not the discharges, with a notable memory saving. In fact the head does not depend on the value of the discharges at the previous step.

The LDG formulation is fully explicit and stability is achieved only by using a small time step. The maximum time step allowed to have convergence depends, among other factors, on the order of the spectral approximation within the elements, decreasing considerably for higher approximations. For the diffusion operator the time step is equal to [8]:

$$\Delta t = C\frac{\Delta x_{\min}^2}{T_{\max} N^4} \tag{21}$$

where $\Delta x_{\min}$ is the smallest side (length) of the elements, $T_{\max}$ is the maximum value of the transmissivity, N is the order of the polynomial approximation, and C is a constant less than one. Herein we use (21) with $C = 0.5$ as the time step for the LDG method.

7. Applications

7.1. Example 1

First we explore the performance of the LDG method in a test example with given analytical solution. The test example has a non-smooth solution that was chosen on purpose to show the advantages and limits of the method when complicated potential head fields are computed. The simulation results are then compared to a priori error estimate derived for smooth solutions [10,11]. We consider an aquifer 100 m × 100 m with a constant transmissivity of 1 m^2/day (Fig. 2a). The corresponding boundary conditions are: fixed head equal to 100 m at the lower side of the domain and fixed head equal to 25 m at the other three sides. For initial conditions we consider a constant head equal to 25 m within the domain. After a transient period, the head distribution in the domain converges to the following steady-state analytical solution, plotted in Fig. 2a [9; p. 147]:

$$h = 25 + \frac{300}{\pi}\sum_{n=0}^{\infty}\frac{1}{(2n+1)}\sin\frac{(2n+1)\pi x}{100} \times \sinh\frac{(100-y)(2n+1)\pi}{100}\operatorname{cosech}(2n+1)\pi \tag{22}$$

In Fig. 2a we note that the jump in the value of the potential head at the boundary results in a folded head surface near the two lower corners. In the following we discuss the advantages and limits of the LDG method applied to this problem, from a water resources perspective. The existence of an analytical solution enables a direct calculation of the error associated with the numerical approximation. To compare the error of the LDG solutions using different polynomial orders and meshes with a different number of elements, we utilize the discrete 2-norm of the error, defined as:

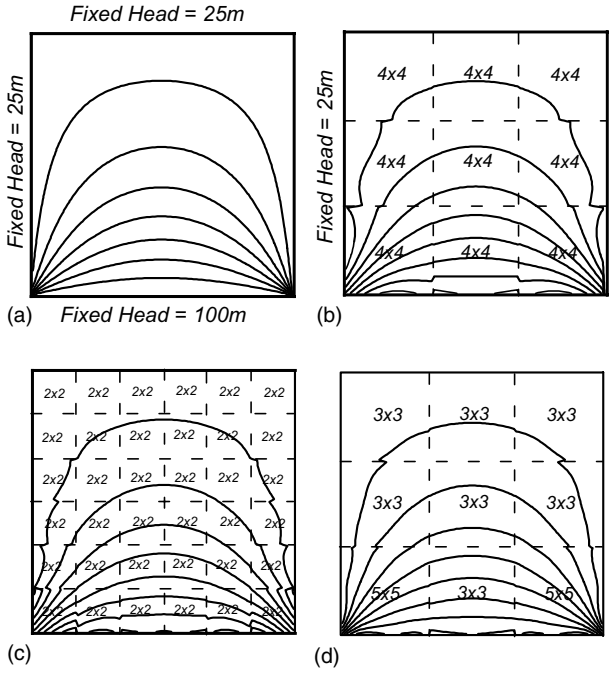

Fig. 2. Steady-state distribution of potential head (isolines) in an aquifer with fixed value of the head at the boundaries. (a) Analytical solution (see Eq. (22)); (b) solution obtained with the LDG method with a mesh of nine elements and a polynomial order equal to 4 in each element; (c) solution obtained with the LDG method with a mesh of 36 elements and a polynomial order equal to 2 in each element; (c) solution obtained with the LDG method with a mesh of nine elements and different polynomial order in each element (the polynomial order is increased in areas where the numerical error is high); the LDG solutions are obtained at steady state.

$$\|\epsilon\|_2 = \sqrt{\frac{\sum_{i=1}^{N} (H_i - h_i)^2}{N}} \tag{23}$$

where H_i is the value of the approximation at the point i and h_i is the pointwise value of the real solution ($\|\epsilon\|_2$ is calculated at the same points in each simulation). We start with a grid with nine elements and a polynomial approximation inside each element of order 2 (nine evaluation points) in both x- and y-direction and we run the model until the steady-state solution is reached. If we want to improve the accuracy of the solution we can either increase the order of the basis functions in each element (p-refinement) or increase the number of elements maintaining the order of the basis functions constant (h-refinement). In Fig. 2b the solution with nine elements and order four is reported, whereas in Fig. 2c the solution with 36 elements and order two is shown. Even though the analytical solution is continuous, both approximations are discontinuous at the elements interfaces. Discontinuities in the solution are particularly evident when the potential head surface is extremely folded, as it is the case at the lower corners of Fig. 1. Here a polynomial surface of high order is necessary to approximate the solution and its steep gradients. The discontinuity of the solution strongly limits the applicability of the LDG method in water resources problems. In fact the same solution calculated with a standard finite-element method is always continuous, since the basis functions are continuous in contiguous elements. This does not necessary mean that the finite-element method is more accurate, but simply that the finite-element method always leads to a continuous solution even with few mesh points. The only way to improve the continuity of the solution with the LDG method is by increasing the polynomial order in the elements until the approximate solution can adequately fit the real solution.

Another fundamental characteristic of the LDG method is the possibility of increasing the order of the basis in each element, without modifying the order in the contiguous elements. This is virtually impossible in finite differences and finite elements where the scheme order is fixed 'a priori' and the only way to improve the accuracy is by increasing the number of elements (h-refinement). In Fig. 2d we increased the basis order in the two critical elements at the lower corners of the domain, producing a noteworthy improvement in the quality of the solution.

Castillo et al. [11] derived a priori error estimate for smooth solutions finding that the error is proportional to h^{k+1} for an h-refinement, where h is the mesh size and k the polynomial order of the approximation. By plotting the error as a function of the degrees of freedom we note that the convergence rate in our example is only one (rather than three) for an h-refinement with polynomials of second order (see Fig. 3), indicating that the convergence rate deteriorates when non-smooth solutions are calculated. Furthermore Castillo et al. [11] showed with numerical examples that a p-refinement leads to exponential convergence. In our simulation a p-refinement (increasing the polynomial order in a mesh

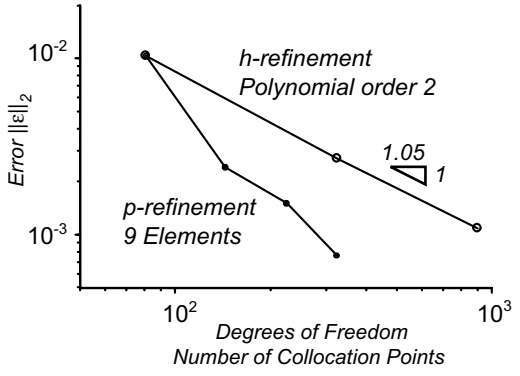

Fig. 3. h-Refinement and p-refinement for the test example shown in Fig. 2. In the h-refinement the polynomial order is maintained constant and equal to two whereas in the p-refinement a fixed mesh with nine elements is used. The convergence rate for the h-refinement is indicated.

with nine elements) shows that the convergence rate is indeed higher than the *h*-refinement, but it is not possible to prove that it is exponential (Fig. 3). In groundwater simulations a *p*-refinement has thus two major advantages: (i) the error is strongly reduced with an increment of the degrees of freedom; (ii) the continuity of the solution is improved (whereas with an *h*-refinement there are more elements that can possibly lead to discontinuities at the interfaces).

A *p*-refinement can be also adaptively applied. The best strategy is to calculate two solutions with two consecutive polynomial orders and then to refine (i.e. increase the order) only where the difference between the two solutions is remarkable.

Since an increase in the polynomial order consistently reduces the error and better preserves the continuity of potential head, in the next examples we mainly focus on the *p*-refinement of the solution.

7.2. Example 2

In the second example we consider a square aquifer (100 m × 100 m) with a constant transmissivity of 1 m^2/day (Fig. 4a).

The corresponding boundary conditions are: fixed head (Dirichlet boundary condition) equal to 10 m for the edges of the element at the lower right corner, fixed head equal to 0 m for the edges of the upper left element, and zero flux for the other boundaries (Neumann boundary condition). Solutions obtained with the LDG model are compared with solutions of the finite-element model MODFE [18,37,38], with the same degrees of freedom (number of nodes or number of evaluation points). Hereafter we refer to this model as FEM. Although both models resolve the parabolic transient flow problem, in this second example we show only results in term of streamlines computed after 24,000 days of simulation, when the solution is close to the final steady state. In this way it is also possible to qualitatively compare our numerical experiments with others dealing with the steady elliptic formulation [19,29].

Starting from initial conditions of zero potential head in the aquifer, the time stepping problem is resolved for 24,000 days. In the spectral approximation the aquifer is divided in 25 square elements (Fig. 4a). The numerical experiment is carried out varying both the order of the approximating polynomial inside each element of the LDG and the number of the nodes for the FEM (Fig. 4b). The coupling of high order basis functions with weak boundary conditions, which characterizes the discontinuous Galerkin formulation, succeeds in resolving the flow problem only when the order of the polynomial is sufficient to approximate the solution. Low order interpolating functions imply poor approximation inside the elements and jumps at the boundaries. Under these circumstances streamlines have spurious

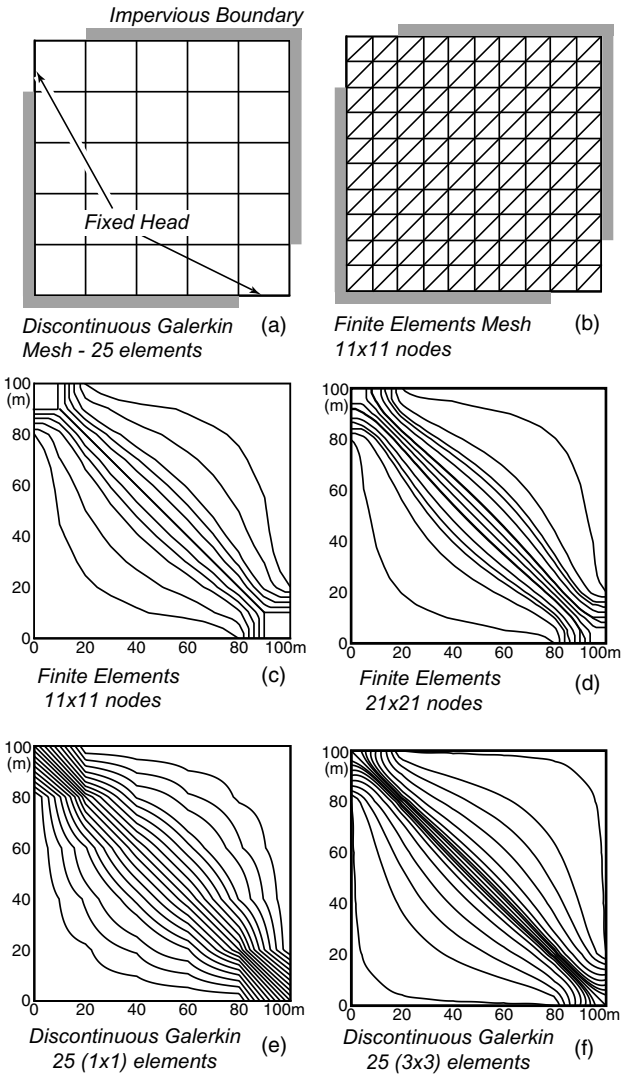

Fig. 4. (a) Quadrilateral mesh for the discontinuous Galerkin; (b) triangular mesh for the finite-elements method. Comparison between streamlines calculated with the FEM and the LDG with different mesh resolution and polynomial order (after 24,000 days of simulation for the aquifer in (a)). (c) FEM 11 × 11 nodes; (d) FEM 21 × 21 nodes; (e) LDG 25 (1 × 1) elements; (f) LDG 25 (3 × 3) elements.

oscillations (Fig. 4e) with angular points at the interfaces of the elements, and the boundary conditions are not well respected. As a consequence the finite-element method with same number of unknowns (nodes) is more accurate (Fig. 4c).

The situation is reversed when the order of the spectral method is increased. In the finite-element method, a linear approximation of the head implies a constant discharge in each element, with abrupt discontinuities from one element to another, and consequently poorly resolved streamlines (Fig. 4d). With a spectral method the approximation of the discharge becomes a polynomial of high order, implying a continuous (non-constant) discharge field in each element. If the solution is smooth enough, the exponential rate of

convergence enhances the quality of the streamlines, for example in both the diverging zone close to the boundaries and in the converging zone close to the diagonal of the aquifer (Fig. 4f). This is in agreement with numerical and theoretical results, stating the high convergence rate for the LDG method [10,11,17].

7.3. Example 3

Factors that cause difficulties and inefficiencies when using spectral methods are irregular domains and variable resolution requirements in different parts of a large domain. The discontinuous Galerkin formulation allows for dividing the domain into elements that follow the domain geometry, and for using a different order of approximation and different transmissivity in each element. In this third numerical experiment we explore the ability of the LDG to deal with discontinuities in permeability. The example aquifer is a square (100 m $\times$ 100 m) and is divided into 25 zones with different transmissivity (Fig. 5a). The transmissivity ranges from 1 to 10^{-2} m^2/day. We impose boundary conditions of zero flux for the upper and lower side of the aquifer, constant head equal to 10 m for the left side and constant head equal to 0 m for the right side. Again, in the first comparison, we consider the streamlines after 24,000 days, close to the steady-state solution.

We utilize the solution obtained with the LDG and polynomial order 9 in the elements for comparison with numerical experiments (Fig. 5b). Because the streamline distribution does not present perceptible differences by increasing the order, we call this solution the 'exact solution'. The LDG formulation is applied to the same problem with different polynomial order in each element (order 2 and order 4 in Fig. 5e and f). Even with a low order approximation, the LDG solution is close to the streamline distribution of the 'exact solution' (compare Fig. 5e and f with Fig. 5b). In contrast, streamlines obtained with the FEM using a number of nodes equal to the number of evaluation points in the LDG approximation exhibit strong discrepancies with the 'exact solution' (Fig. 5c and d). With the spectral method, however, problems can arise when imposing boundary conditions. On the one hand, the weak formulation utilizing fluxes at the element boundaries greatly increases the flexibility of the method in separating the domain into elements, but on the other hand it does not ensure a rigorous treatment of the boundary conditions. The head values at the Dirichlet boundaries are not enforced directly as in the finite-element method; rather they are transformed into an integral flux. Discrepancies between the boundary conditions and the approximated solution can occur for low approximation order. Similarly, the zero-flux boundary condition is enforced in an integral form, and local (albeit small) normal discharges can appear. A direct consequence is

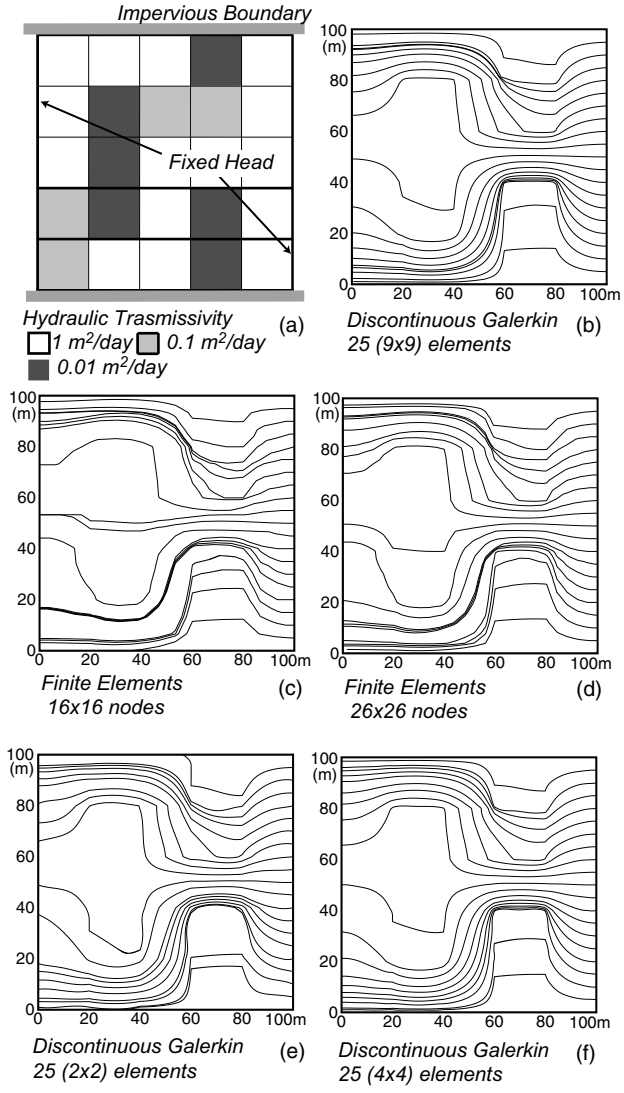

Fig. 5. (a) Aquifer with differences in transmissivity; (b) corresponding streamlines calculated with the LDG method with polynomial order equal to 9 after 24,000 days of simulation (called the 'exact solution'); comparison between streamlines calculated with the FEM and the LDG method with different mesh resolution and polynomial order (after 24,000 days of simulation for the aquifer in (a)). (c) FEM 16$\times$16 nodes; (d) FEM 26$\times$26 nodes; (e) LDG 25 (2$\times$2) elements; (f) LDG 25 (4$\times$4) elements.

that with a low order approximation, streamlines can cross the impervious boundaries (Fig. 5e).

In this section we have compared two codes for the time-dependent formulation of the flow. Time stepping methods are usually selected to achieve some prescribed accuracy at the lowest cost—that is, to minimize the product of the cost per time step and the number of time steps needed. These methods are either explicit or implicit, emphasizing speed per time step or minimizing the number of time steps respectively. The finite-element code MODFE utilizes the Modified Incomplete-Cholesky Conjugate-Gradient (MICCG) and an implicit, first order algorithm for the time integration [18]. The

method is unconditionally stable, but a time step that is too large can cause the temporal error to dominate, particularly in the first part of the transient simulation. When the system reaches the steady state, the temporal error decays because the solution becomes independent of time, and the spatial error is dominant.

We then compare the error of the LDG method using different polynomial orders (p-refinement) with the error of the FEM method. The error is calculated by using Eq. (23), evaluated on N points chosen as the centers of the triangles of a finite-element mesh with 201×201 nodes. Since the analytical solution of the case studied does not exist, we compare each approximation with the 'exact solution' reported in Fig. 5b.

The discrete 2-norm of the discharge error for several LDG and FEM solutions is plotted in Fig. 6a and b as a function of the degrees of freedom after 24,000 days, when the system is very close to steady conditions. For both the x-component and y-component of the discharge the convergence rate (slope of the line) is higher for the spectral method than for the finite-elements method (Fig. 6a and b). Since the simulation is time-dependent, the same comparison is performed after 2000 days, when the head transient is passing through the central strong heterogeneity region in Fig. 5a. Again the convergence rate is higher for the spectral method (Fig. 6c and d). In this test case the p-refinement of the LDG method does not show exponential convergence, as it is the case for smooth solutions [11], since the discontinuities in transmissivity degrade the convergence rate of the solution. Despite the lack of exponential convergence, a p-refinement with the LDG method is more accurate than the FEM method with the same number of degrees of freedom. However, the advantages of a more accurate solution can be undermined by a dramatic increase in the utilization of CPU time and computer memory.

With the aim of comparing the performance of the two methods with respect to the CPU time, we must first consider the "correct" choice of the time step for the implicit finite-element algorithm. A time step that is too large, even if it allows to compute the solution utilizing less CPU time, can involve a temporal error which compromises the accuracy of the method. This is particularly evident during the first part of the simulation, where the time dependence is very strong. In Fig. 7a, for the FEM, the error is plotted as a function of the ratio between the time step Δt and the mesh size Δx after 240 days. Because the finite-element method is second order in space for the head, it follows that it is first order for the discharges. The method is also first order in time, so the error scales with the ratio $\Delta t/\Delta x$. The left part of Fig. 7a shows that for small time steps the spatial error dominates whereas for large time steps the temporal error is predominant. A value of $\Delta t = 2\Delta x$ reasonably divides the two zones, and represents the maximum

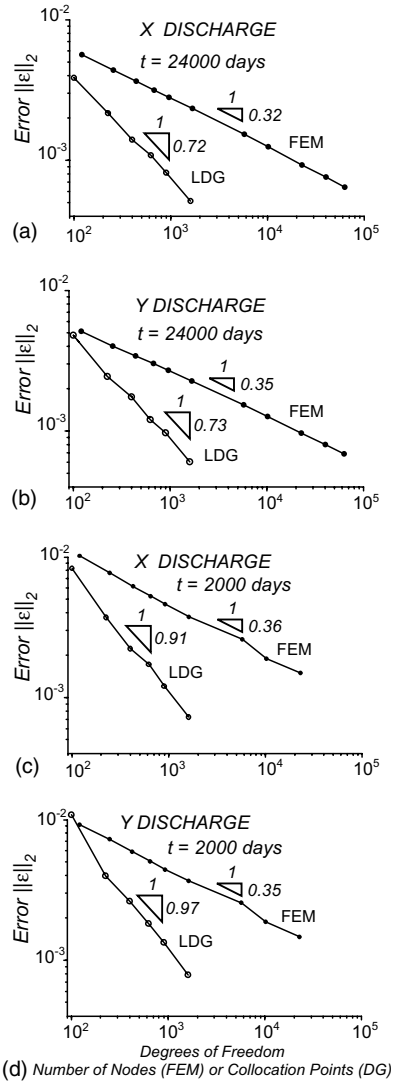

Fig. 6. Discrete 2-norm of the error (assuming the LDG with order 9 as the exact solution) for several simulations utilizing the LDG method with different polynomial order and the FEM with different number of nodes; (a) x-discharge; (b) y-discharge. The 2-norm is calculated for the discharge components for the problem of Fig. 5a (after 24,000 days of simulation). Discrete 2-norm of the error calculated for the discharge components for the problem of Fig. 5a after 2000 days of simulation; (c) x-discharge; (d) y-discharge.

allowable time step without incurring large temporal errors. For the FEM method we then use a timestep $\Delta t = 2\Delta x$, with Δx the mesh size.

In Fig. 7b we report results obtained by running the two codes with different numbers of degrees of freedom on an Origin 200 s at 180 MHz. The CPU time for each simulation is plotted as a function of the error (as previously defined) after 24,000 days of simulation. The CPU time required for the two methods is of the same order of magnitude, and the LDG method is advantageous when a small final error is required. The higher accuracy of the spectral method can then justify the higher computational cost.

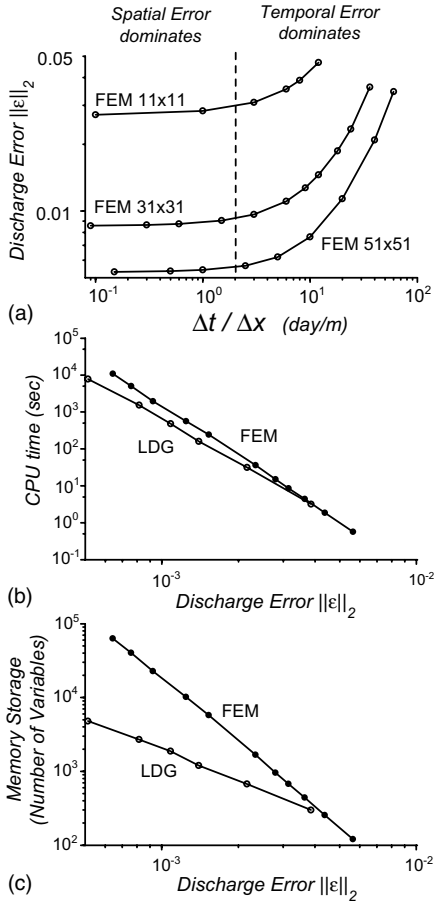

Fig. 7. (a) Error for the x discharge calculated using the FEM with different meshes as a function of the ratio between time step and spatial step. The results are calculated after 240 days of simulation. The dashed line corresponds to a time step equal to twice the spatial step; (b) CPU time as a function of the discharge error for several LDG and FEM simulations; (c) memory storage as a function of the discharge error calculated with the 2-norm for several LDG and FEM simulations.

However this result has to be judged only qualitatively. Usually we are interested in modeling the evolution of features at a time scale longer than the time scale of the potential head diffusion across a cell. If this is the case implicit methods as the program MODFE are certainly more efficient. Furthermore, caution should be exercised in interpreting CPU times based on different computer models, as programming techniques may influence CPU times.

A recent implicit implementation of the LDG method [34] using a matrix-free Newton–Krylov–Schwarz algorithm can further improve the efficiency of the LDG method. Results presented in Rasetarinera and Hussaini [34] show that the implicit formulation is 50 times faster than the explicit method herein presented.

The superiority of the LDG method is instead completely manifest in the memory storage. Few evaluation points and a suitable interpolation in the LDG give the same accuracy of a FEM with many more nodes. Even if we consider the total number of variables that we have to store in the LDG method (i.e. head, x and y discharges) the comparison is in favor of the spectral approximation (Fig. 7c). However, nowadays memory storage is of minor importance given the availability and low cost of computer memory.

7.4. Example 4

In the fourth example the LDG method is compared to the hybrid finite-element method described in Mosé

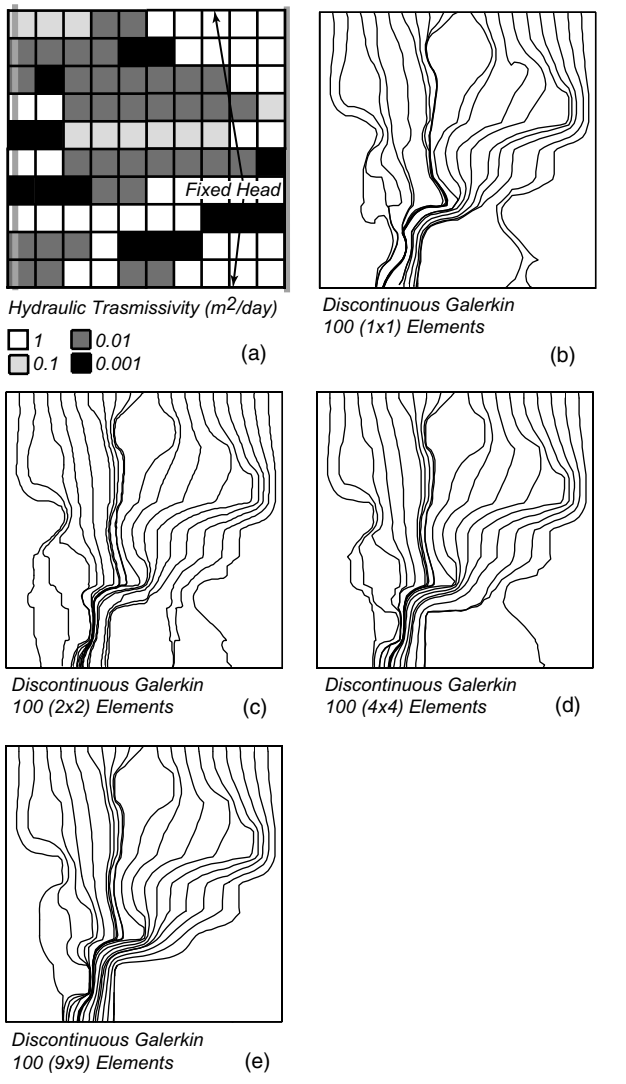

Fig. 8. (a) Aquifer with transmissivity ranging from 0.001 to 1 m^2/s. The same example was used in Mosé et al. [29] to study the accuracy of the mixed finite-elements method; (b) streamlines for the aquifer of figure (a) calculated with the LDG method and order basis one (steady state); (c) streamlines calculated with the LDG method with order basis two after 50,000 days of simulation; (d) streamlines calculated with the LDG method with order basis four; (e) streamlines calculated with the LDG method with order basis nine. These results can be directly compared with the results reported in Mosé et al. [29] (see the text for a discussion).

et al. [29]. In the hybrid finite-element method the potential head and the discharges are simultaneously calculated and satisfy an exact water balance in each element. This formulation overcomes the problem of standard finite elements where the velocity is discontinuous at the element boundaries, reducing the accuracy in the calculation of the discharges (see Example 3).

We utilize the same domain described in Fig. 16 of Mosé et al. [29]. A squared aquifer with side dimension of 100 m is divided into 100 elements with transmissivity ranging from 1 to 0.001 m^2/day (Fig. 8a). The head at the higher and lower sides of the domain is kept constant and equal to 100 and 90 m respectively, whereas the lateral sides are set as impermeable (zero flux). Since the solution derived in Mosé et al. [29] was calculated resolving the steady-state problem, we utilize our time-dependent method with an initial condition of 90 m everywhere, and we run the model until it reaches the final steady-state solution. The solutions of the two methods can thus be qualitatively compared.

Once again we increase the order of the basis in each element of the LDG, since we have already shown that a *p*-refinement is more efficient than an *h*-refinement. Solutions with polynomial order one, two, four, and nine are reported in Fig. 8b–e respectively. A comparison with the results showed in Mosé et al. [29] reveals that only the solution with order nine realistically approximates the exact solution, whereas in the other approximations the resulting streamlines are poorly resolved. It is important to note that Mosé et al. [29] already obtain accurate streamlines with mesh 40×40 (4800 unknowns), whereas the solution with the LDG method with 100 elements of order 4 (7500 unknowns) is still inaccurate in terms of streamlines. Thus the superiority of the mixed finite-element method is fully manifest when few degrees of freedom are used.

8. Conclusions

We applied the discontinuous spectral Galerkin method to the groundwater flow problem and compared the results with those obtained by a standard finite-element and a mixed finite-element method. The discontinuous spectral Galerkin method provides highly accurate results for the discharge field with a reasonable CPU time. The following conclusions have been derived from the simulations presented in this paper: (i) With the discontinuous spectral Galerkin method it is possible to improve the accuracy of the solution by increasing the number of elements (*h*-refinement) of the polynomial order inside each element (*p*-refinement). In aquifers with homogeneous transmissivity the convergence rate with a *p*-refinement is higher than the convergence rate with an *h*-refinement. (ii) When the method is applied to aquifers with a complex distribution of potential head, the discontinuous formulation produces jumps at the element boundaries, particularly when low order polynomial basis functions are used. To circumvent this problem the approximation order needs to be increased in areas where the potential head surface is extremely folded. (iii) The discontinuous formulation makes it possible to locally increase the order of the elements. This is the major advantage of the scheme, which provides extreme flexibility when complex flows are studied (a local *p*-refinement is not possible with finite elements, and finite differences). (iv) The weak formulation utilized to match the different elements can produce poor results at the boundaries, especially when low order polynomials are utilized in the presence of non-smooth solutions. (v) The discontinuous formulation is particularly effective in aquifers with differences in transmissivity, where it is possible to assign different elements to zones with different transmissivity. (vi) Comparison between the LDG method and the standard FEM in a aquifer with differences in transmissivity proves that the LDG method with a *p*-refinement has a higher convergence rate than the standard FEM. However the convergence rate is not exponential because of differences in transmissivity. For a given accuracy, the method requires far fewer evaluation points than the finite-element method. (vii) Comparison between the LDG and the mixed finite-elements method in an aquifer with differences in transmissivity clearly shows that the mixed finite-element method is superior, especially when low order polynomials are utilized in the LDG.

We then conclude that the LDG method is suitable for the calculation of the groundwater flow field in applications that require a very high accuracy, for which the high order of the approximation and the high convergence rate are necessary. The discontinuous formulation allows to assign a different transmissivity to each mesh element, favoring the application of the scheme to heterogeneous aquifers. Once the transmissivity field is assigned, it is more efficient to increase the polynomial order (*p*-refinement) rather than to increase the number of elements (*h*-refinement) in each aquifer zone. Since the performance of the method increases when high order elements are used, it is preferable to apply the LDG method to aquifers that are divided in few zones with different transmissivity, rather to aquifers with a high heterogeneous transmissivity field. Finally the simulations presented in this paper can be viewed as a benchmark for a coupled flow field and mass transport spectral model.

Acknowledgements

We thank two anonymous reviewers and David Kopriva for their comments and suggestions. The manuscript greatly benefited from them.

References

[1] Abramowitz M, Stegun I. Handbook of mathematical functions. Mineola, New York: Dover; 1972.

[2] Aizinger V, Dawson C, Cockburn B, Castillo P. The local discontinuous Galerkin method for contaminant transport. Adv Water Resour 2000;24(1):73–87.

[3] Arnold DN, Brezzi F, Cockburn B, Marini D. Discontinuous Galerkin methods for elliptic problems. In: Cockburn B, Karniadakis G, Shu CW, Griebel M, editors. Discontinuous Galerkin methods: theory, computation and applications. Lecture notes in computational science and engineering. Springer Verlag; 2000.

[4] Arnold DN, Brezzi F. Mixed and nonconforming finite element methods: implementation, postprocessing and error estimates. Math Modell Numer Anal 1985;19:7–32.

[5] Bellin A, Salandin P, Rinaldo A. Simulation of dispersion in heterogeneous porous formations: statistics, first-order theories, convergence of computations. Water Resour Res 1992; 28(9):2211–27.

[6] Bear J, Verruijt A. Modeling groundwater flow and pullution. Dordrecht: Reidel; 1987.

[7] Brezzi F, Manzini M, Marini D, Pietra P, Russo A. Discontinuous finite elements for diffusion problems. In: Francesco Brioschi (1824–1897) Convegno di Studi Matematici, October 22–23, 1997. Ist Lomb Acc Sci Lett, Incontro di studio no 16, 1999. p. 197–217.

[8] Canuto C, Hussaini MY, Quarteroni A, Zang TA. Spectral methods in fluid dynamics. Berlin: Springer-Verlag; 1988.

[9] Carslaw HS, Jaeger JC. Conduction of heat in solids. Oxford: Clarendon Press; 1959. 510 pp.

[10] Castillo P. An optimal estimate for the local discontinuous Galerkin method. In: Cockburn B, Karniadakis G, Shu CW, Griebel M, editors. Discontinuous Galerkin methods: theory, computation and applications. Lecture notes in computational science and engineering. Springer Verlag; 2000.

[11] Castillo P, Cockburn B, Schotzau D, Schwab C. Optimal a priori error estimates for the hp-version of the local discontinuous Galerkin method for convection–diffusion problems. Math Comput 2002;71(238):455–78.

[12] Chavent G, Roberts JE. A unified physical presentation of mixed, mixed hybrid finite elements and standard finite difference approximations for the determination of discharges in waterflow problems. Adv Water Resour 1991;14(6):329–48.

[13] Cirpka OA, Frind EO, Helmig R. Streamline-oriented grid generation for transport modelling in two-dimensional domains including wells. Adv Water Resour 1999;22(7):697–710.

[14] Cockburn B, Shu CW. TVB Runge–Kutta local projection discontinuous Galerkin finite-element method for conservation-laws. 2. General framework. Math Comput 1989;52(186):411–35.

[15] Cockburn B, Lin SY, Shu CW. TVB Runge–Kutta local projection discontinuous Galerkin finite-element method for conservation-laws. 3. One-dimensional systems. J Comput Phys 1989; 84(1):90–113.

[16] Cockburn B, Hou SC, Shu CW. The Runge–Kutta local projection discontinuous Galerkin finite-element method for conservation-laws. 4. The multidimensional case. Math Comput 1990; 54(190):545–81.

[17] Cockburn B, Shu CW. The local discontinuous Galerkin method for time-dependent convection-diffusion systems. SIAM, J Numer Anal 1998;35(6):2440–63.

[18] Cooley RL. A MODular Finite-Element model (MODFE) for areal and axisymmetric ground-water-flow problems, part 2—derivation of finite-element equations and comparisons with analytical solutions. US Geological Survey Techniques of Water-Resources Investigations. Book 6, 1992 [chapter A4].

[19] Cordes C, Kinzelbach W. Continuous groundwater discharge field and path lines in linear, bilinear, and trilinear finite elements. Water Resour Res 1992;28(11):2903–11.

[20] Cordes C, Kinzelbach W. Comment on "Application of the mixed hybrid finite element approximation in a groudwater flow model: Luxury or necessity?" by R. Mosé, P. Siegel, P. Ackerer and G. Chavent. Water Resour Res 1996;32(6):1905–9.

[21] Durlofsky LJ. Accuracy of mixed and control volume finite element approximations to Darcy discharge and related quantities. Water Resour Res 1994;30(4):965–73.

[22] Frind EO, Matanga GO. The dual formulation of flow for contaminant transport modeling, 1, Review of theory and accuracy aspects. Water Resour Res 1985;21(2):159–69.

[23] Goblet P, Cordier E. Solution of the flow and mass transport equations by means of spectral elements. Water Resour Res 1993;29(9):3135–44.

[24] Hussaini MY, Kopriva DA, Patera AT. Spectral collocation methods. Appl Numer Math 1989;5(3):177–208.

[25] Karniadakis GE, Sherwin SJ. Spectral/hp element methods for CFD. New York: Oxford University Press; 1999.

[26] Kopriva DA, Woodruff SL, Hussaini MY. Computation of electromagnetic scattering with a non-conforming discontinuous spectral element method. Int J Numer Meth Eng 2002;53(1): 105–22.

[27] Matanga G. Stream functions in three-dimensional groundwater flow. Water Resour Res 1993;29(9):3125–33.

[28] Meissner U. A mixed finite element model for use in potential flow problems. Int J Numer Methods Eng 1973;6:467–73.

[29] Mosé R, Siegel P, Ackerer P, Chavent G. Application of the mixed finite element approximation in a groundwater flow model: luxury or necessity? Water Resour Res 1994;30(11):3001–12.

[30] Oden JT, Babuska I, Baumann CE. A discontinuous hp finite element method for diffusion problems. J Comput Phys 1998; 146(2):491–519.

[31] Patera AT. A spectral element method for fluid dynamics: laminar flow in a channel expansion. J Comput Phys 1984;54:468–88.

[32] Pinder G, Gray W. Finite element simulation in surface and subsurface hydrology. New York: Academic Press; 1977.

[33] Pollock DW. Semianalytical computation of pathlines for finite difference models. Ground Water 1988;26(6):743–50.

[34] Rasetarinera P, Hussaini MY. An efficient implicit discontinuous spectral Galerkin method. J Comput Phys 2001;172(2):718–38.

[35] Riviere B, Wheeler MF, Banas K. Part II. Discontinuous Galerkin method applied to a single phase flow in porous media. Comput Geosci 2000;(4):337–49.

[36] Salandin P, Fiorotto V. Solute transport in highly heterogeneous aquifers. Water Resour Res 1998;34(5):949–61.

[37] Torak LJ. A MODular Finite-Element model (MODFE) for areal and axisymmetric ground-water-flow problems, part 1—model description and user's manual. US Geological Survey Techniques of Water-Resources Investigations. Book 6, 1993 [chapter A3].

[38] Torak LJ. A MODular Finite-Element model (MODFE) for areal and axisymmetric ground-water-flow problems, part 3—design philosophy and programming details. US Geological Survey Techniques of Water-Resources Investigations. Book 6, 1993 [chapter A5].

[39] Shu CW, Osher S. Efficient implementation of essentially non-oscillatory shock-capturing schemes. J Comput Phys 1988;77: 439–71.